Available online at www.sciencedirect.com
ScienceDirect
Journal of Solid State Chemistry 180 (2007) 2400–2408
JOURNAL OF SOLID STATE CHEMISTRY
www.elsevier.com/locate/jssc

Photoluminescence and structural characteristics of $Lu_2O_3:Eu^{3+}$ nanocrystallites in silica matrix

Jerzy Sokolnicki

Faculty of Chemistry, University of Wrocław, 14 F. Joliot-Curie Street, 50-383 Wrocław, Poland

Received 14 February 2007; received in revised form 12 June 2007; accepted 20 June 2007
Available online 23 June 2007

Abstract

Two silica ceramics were obtained by mixing nanocrystalline $Lu_2O_3:Eu^{3+}$ with silica sol using the sol–gel technique. The synthesis procedure for both samples differed in the pH of the sol and time of the sol condensation before substrates were mixed together, which implied their different optical properties. The first one has the same spectroscopic properties as $Lu_2O_3:Eu^{3+}$ nanocrystallites with an exception of small lowering of the charge transfer (CT) band intensity. This feature is preserved up to about 950 °C. Above this temperature, nanocrystallites of $Lu_2O_3:Eu^{3+}$ react with the silica matrix synthesis pyrosilicate ($Lu_2Si_2O_7$). The Eu^{3+} ions occupy only one crystallographic site in the crystal lattice for low concentration of the activator (1%) and two sites for higher concentration (10%). The second sample exhibits different Eu^{3+} emission than $Lu_2O_3:Eu^{3+}$ nanocrystallites and, additionally, a broad band of the matrix originating at the green region of the spectrum. Sintering the sample at higher temperatures leads to disappearance of this broad emission and continuous changes of the Eu^{3+} emission because of the progressive conversion of the $Lu_2O_3:Eu^{3+}$ to pyrosilicate. At 1300 °C for both samples, the reaction of synthesis lutetium pyrosilicate is completed. Structural characteristic of the samples is presented and correlate with the decay profile of the Eu^{3+} emission.

Keywords: Photoluminescence; Lutetium oxide; Lutetium pyrosilicate; Nanocrystallites; Sol–gel technique

1. Introduction

The need for new phosphors for high-resolution X-ray imaging systems underlies wide investigations towards improving their scintillation performances and preparation techniques [1–3].

Widely investigated lutetium oxide doped with rare earth ions, is considered to be one of the most promising materials for X-ray detection [4]. There are numerous methods for forming metal oxide nanoparticles, among others precipitation followed by a thermal decomposition [5], combustion synthesis [6] and sol–gel processing [7–11].

Lu_2O_3 crystallizes in a cubic C-type structure [12–14] and offers two different sites for the metal ions, one with C_2 and one with S_6 symmetry. The former site lacking inversion center is quite favorable for observing the electric dipole transition as a forced transition due to the admixture of the odd parity states. The latter is unfavorable for the electric dipole transition due to the presence of the inversion center and only show magnetic dipole emission [12,14].

Nanoscale materials are known to exhibit changed physical properties of the host, which affects the luminescence and dynamics of an optically active dopant. Investigation and comprehension of these materials is important for optimizing their optical properties for technological applications in communication and display devices. Preparing lanthanide-doped nanostructures also gives a possibility to develop and study transparent composite materials. Nanometer-sized particles exhibit reduced optical scattering, allowing the preparation and use of nanocrystals embedded in an amorphous matrix in applications such as laser and amplifiers, which usually require high-quality crystals or glasses. Such ceramics in the form of thin films [2,15] and as a bulk [16], obtained by the sol–gel method, have recently proved to be very promising for scintillation application. Also, the recently developed inorganic scintillator, Ce^{3+} doped $Lu_2Si_2O_7$, has been lately studied due to promising performance for

E-mail address: sj@wchuwr.pl

0022-4596/$ - see front matter © 2007 Elsevier Inc. All rights reserved.
doi:10.1016/j.jssc.2007.06.015

applications such as emission tomography or oil well logging [17,18].

$Lu_2Si_2O_7$ crystallizes in a monoclinic structure, with the space group $C2/m$(no. 12) [19]. The structure may be considered as a distorted hexagonal packing of oxygens containing the lutetium atoms in octahedral sites, and the silicon ions in tetrahedral ones, in alternating layers [20]. Three types of oxygen can be distinguished: the first one (O1) is a bridging oxygen between the two silicon ions of the $[Si_2O_7]^{6-}$ group and it is not lutetium bound. The other two oxygen ions (O2 and O3) are terminal oxygen of the $[Si_2O_7]^{6-}$ group and they are involved in lutetium surrounding. The lattice offers only one crystallographic site for doping lanthanide ion.

This paper is devoted to the spectroscopic investigation of two sol–gel derived ceramics, from which one exhibits the same optical properties as Lu_2O_3:Eu^{3+} nanoparticles up to 950 °C of heating and the second is a quite new material. These differences arise from changes in the preparation procedure. It is shown that at 1300 °C for both samples, lutetium oxide is fully transformed to nanocrystalline $Lu_2Si_2O_7$.

2. Experimental

Lu_2O_3:Eu^{3+} containing 1 and 10 mol% of active ions with respect to Lu have been prepared using novel solution combustion synthesis involving a mixed fuel containing glutamic acid and glycine [21]. Stoichiometric quantities of the metal nitrates and fuel (glycine/glutamic acid) were dissolved in a small amount of water in a beaker. Afterwards, the solution was dried at 150 °C for about 3 h. The obtained material was transferred into a furnace preheated up to 600 °C (Carbolite chamber furnace RHF 16/15) and fired for 2 h in air in order to decompose the residual nitrate ions.

Silica sols were obtained by acid-catalyzed hydrolysis of tetraethoxysilane (TEOS) with de-ionized water and addition of C_2H_5OH to allow dissolving of TEOS. The pH were adjusted to 0.5 and 2 by diluted nitric acid. The molar ratios [TEOS]:[H_2O]:[ethanol] were 1:4:8.

Sample (1): The sol of lower pH (0.5) was allowed to condense at room temperature by 72 h. Then, the Lu_2O_3:Eu^{3+} nanocrystalline powder was introduced to the sol and stirred well. The mixture was placed in a polyethylene container and left to gelate at room temperature under a parafilm cover for 3 days. Then, the cover was removed and the sample underwent further condensation and drying for 2 weeks at room temperature.

Sample (2): The sol of higher pH (2.0) was mixed with Lu_2O_3:Eu^{3+} directly after hydrolysis had been finished and allowed to gelate in a polyethylene container under a parafilm cover by three days and then condensed and dried for 2 weeks uncovered. Both sols have been mixed with lutetium oxide containing low and high concentration of active ions.

The xerogel specimens were opaque and disc shaped with 5 mm in diameter and 1 mm in thickness. Cracks did not occur up to 1300 °C.

2.1. Apparatus

Emission spectra were measured using Spectra Pro 750 monochromator, equipped with Hamamatsu R928 photomultiplier and 1200 l/mm grating blazed at 500 nm. The 450 W xenon arc lamp was used as an excitation source. It was coupled with 275 mm excitation monochromator, which used a 1800 l/mm grating blazed at 250 nm. Excitation spectra have been corrected for the excitation light intensity while emission spectra were not corrected for the instrument response. The measurements were done at room temperatures and at 77 K.

Emission kinetics was measured with a Tektronix TDS 3052B oscilloscope and Nd:YAG Lambda Physics pulsed laser.

The ambient temperature Raman spectra were measured with the Bruker RFS 100 FT-Raman spectrometer using the back scattering arrangement. The resolution was 2 cm^{-1}. For excitation, the 1064 nm line of Nd:YAG laser was used.

X-ray analysis was performed with a DRON-1 diffractometer, using Cu$K\alpha$ radiation ($\lambda = 1.5418$ Å) filtered with Ni. The diffractograms were recorded with a step of $2\theta = 0.1°$ for the range of $2\theta = 10$–$120°$. The Scherrer's relation, Eq. (1), was used to estimate the crystallites size,

$$D = \frac{0.9\lambda}{\cos\theta\sqrt{\beta^2 - \beta_0^2}}. \quad (1)$$

In this equation, D is an average crystallite size, λ denotes the X-ray radiation wavelength, β represents a full-width at half-maximum of a diffraction line located at θ and β_0 represents a scan aperture of the diffractometer.

X-ray excited emissions were recorded using the white X-ray radiation from a Cu lamp of a DRON-1 diffractometer, the same one which was used for XRD measurements. The spectra were recorded in a reflection geometry using an Ocean Optics HR2000CGUV-NIR spectrometer equipped with a 600 μm fiber optic and a 25 μm slit. The spectrometer resolution was about 1.3 nm.

3. Results and discussion

All of the crystalline samples obtained were single phase, and the diffraction patterns obtained could be indexed according to the following card numbers: Lu_2O_3—JCPDS card 12-0728, $Lu_2Si_2O_7$—JCPDS card 35-0326, crystobalite of type C—JCPDS card 11-0695. A quantitative line-broadening analysis of the diffraction peaks indicates a crystallite average dimension in the range 20–25 nm for theLu_2O_3 nanocrystallites (planes 222, 400, 440). The nanocrystallites of Lu_2O_3 mixed with silica sol have the same dimensions up to 550 °C, whereas treated at higher

temperatures increase in size and their dimensions are in the range 25–30 nm at 950 °C and 35–40 nm at 1300 °C (pyrosilicate, planes 110, 201, 131).

Fig. 1 presents $^5D_0 \rightarrow {}^7F_J$ emission spectra of the sample (1), taken at 77 K under 250 nm excitation. The spectra measured for the sample before heat treatment and heated up to 950 °C exhibit almost the same characteristic features (band positions, shape, number of components, intensity ratios) as the spectrum of nanocrystalline $Lu_2O_3:Eu^{3+}$. This obviously shows very weak $Lu_2O_3:Eu^{3+}$–SiO_2 host lattice interactions. It is what we expected, as for this sample $Lu_2O_3:Eu^{3+}$ was mixed with the sol after a couple of days from the sol forming. After this time, the sol should be condensed to such an extent that its susceptibility to react with lutetium oxide is very low. Please note that for this sample the pH was lower (0.5) to accelerate condensation of the sol and to ensure that gelation will not occur before mixing the sol with lutetium oxide [22]. We can assume that $Lu_2O_3:Eu^{3+}$ molecules are located in the cavities of porous silica and chemical bondings between them and the lattice are not created. In the process of heating, the residual organic molecules are burnt out, most of the water molecules are removed and the host lattice evolves to SiO_2, simultaneously shrinking. We can presuppose that at 950 °C the matrix is fully densified and consists of almost pure SiO_2 network. Moreover, during heating SiO_2 gradually loses its porous character and becomes a glassy material. Heating the sample beyond this temperature is very likely to produce a new material as a result of the reaction of SiO_2 with the $Lu_2O_3:Eu^{3+}$. The spectrum of the sample heated at 1300 °C is a good confirmation of this presumption. It differs distinctly from those of lower temperatures with respect to intensity ratios and the number of components of respective transitions. Note that the lines are still very narrow showing the crystalline character of the new phase. For such materials, amorphous surrounding of the active ions is more typical [13,23–26]. It results in an inhomogeneous broadening of the emission lines because of the presence of many different environments of the Eu^{3+} ions in the amorphous host.

Fig. 2 shows the excitation spectra of the respective emissions shown in Fig. 1, normalized to the hypersensitive transition ($^7F_0 \rightarrow {}^5D_2$). The spectra taken for the sample heated up to 950 °C have the same band positions, the number of components and their shapes, but differ to some extent in intensity ratios. The charge transfer (CT) band located at about 250 nm, dominates the spectra and exhibits the highest intensity for nanocrystalline $Lu_2O_3:Eu^{3+}$. In silica matrix, its intensity decreases, less for the sample heated at higher temperatures. Please also note that *f–f* transitions located in the UV region of the spectrum are weaker in intensities for the $Lu_2O_3:Eu^{3+}/SiO_2$ samples.

To understand the above facts, one has to take into account that the silica gel or glass cannot be considered as optically inert. It is well known that silica sol–gel derived materials have a potential to absorb the light in the UV, causing some dissipation of the excitation energy. The scale of this dissipation depends on how much the host absorption band overlaps the CT band of Eu^{3+}. The spectral position and intensity of the matrix absorption is in turn influenced by the synthesis conditions, in particular

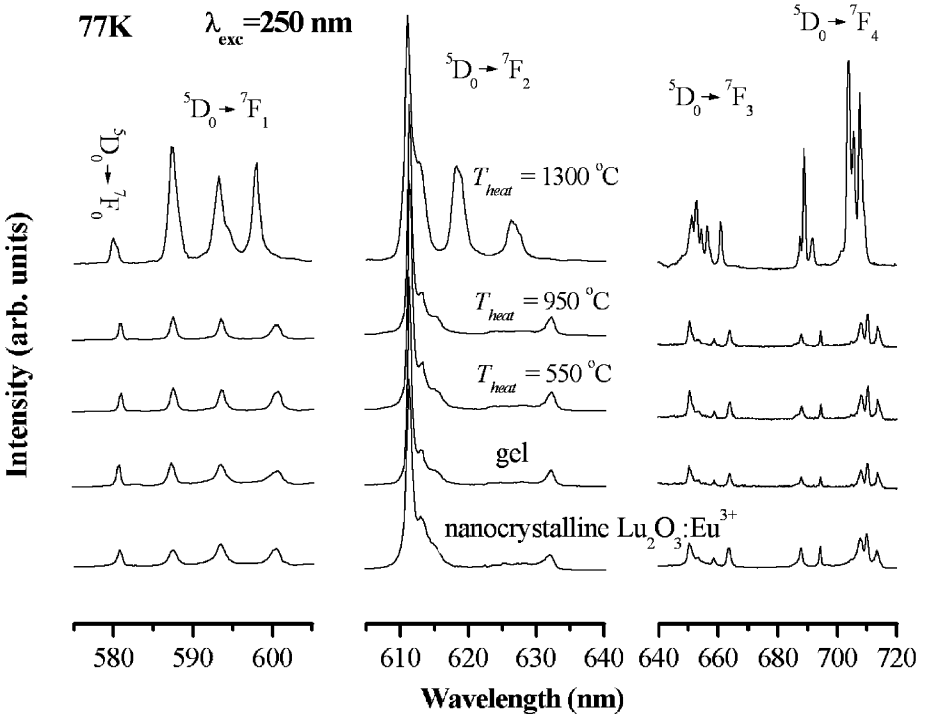

Fig. 1. Luminescence spectra of the sample (1) treated at different temperatures. The spectrum of nanocrystalline $Lu_2O_3:Eu^{3+}$ is included for comparison.

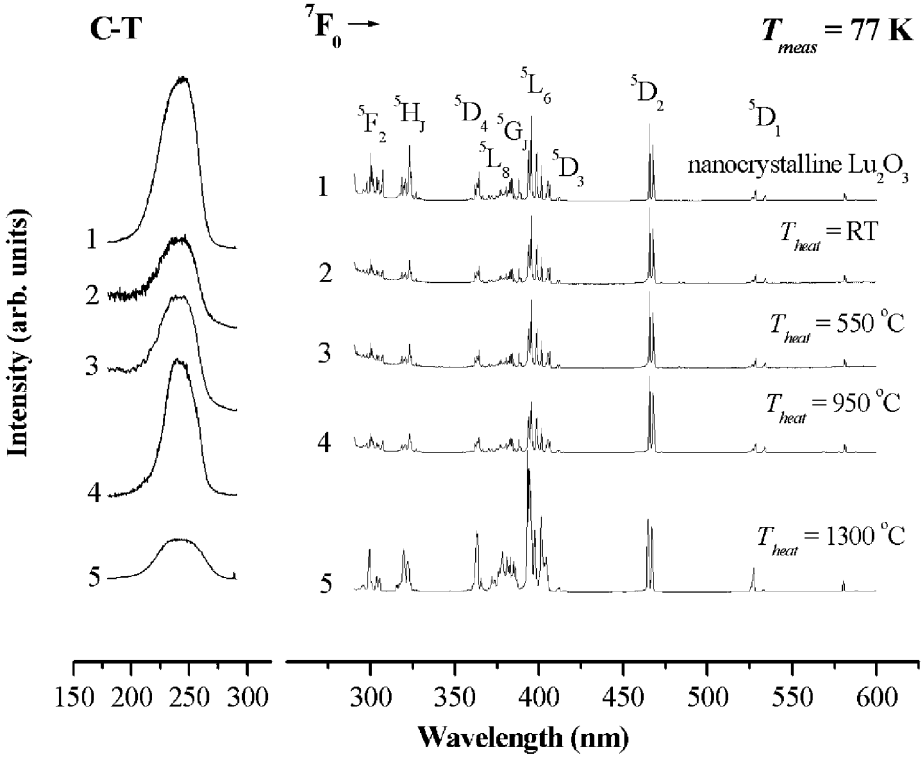

Fig. 2. Excitation spectra of the sample (1) treated at different temperatures. The spectrum of nanocrystalline Lu_2O_3:Eu^{3+} is included for comparison.

the sintering temperature. At 950 °C, the host lattice contains much less isolated Si–OH groups and is almost free of residual organic and water molecules that can trap the energy transferred from the CT state to the excited *f*-levels of Eu^{3+} [22,27]. It is worth noting that the increasing temperature also diminishes the energy dissipation within nanocrystalline Lu_2O_3:Eu^{3+} [28]. Therefore, the CT bands in the spectrum of samples unheated and heated at 550 °C have smaller intensity than for the sample sintered at 950 °C. It should be noted that for the sample (1), the matrix emission has not been observed, independently of the heating temperature. The spectrum of the sample heated at 1300 °C differs from the others for the same reason as mentioned above in case of emission spectrum, that is the formation of Lu_2Si2O_7.

The crystal structure of the sample was examined by XRD and the XRD pattern of the sample heated at different temperatures is shown in Fig. 3. The difractogram of Lu_2O_3:Eu^{3+} nanocrystals is included for comparison. As can be observed, the spectra for the sample heated up to 950 °C show the presence of crystalline lutetium oxide, confirming that Lu_2O_3 does not react with SiO_2 up to this temperature. The spectrum of the sample heated at 1300 °C demonstrates that lutetium oxide is fully transformed to $Lu_2Si_2O_7$ by the reaction with SiO_2. Formation of pyrosilicate in the Nd^{3+} doped sol–gel derived material was previously reported by Legendziewicz [29]. The excess of SiO_2 underwent transformation to crystobalite. Moreover, there is no other crystalline phase containing Ln^{3+} ions which is in agreement with the emission spectra of the relative samples. Maier et al. [30] reported for 1350 °C the coexistence of disilicate and monosilicate that was used as a proof of two steps reaction of disilicates synthesis:

$$RE_2O_3 + SiO_2 \rightarrow RE_2SiO_5, \quad (2)$$

from which disilicates are formed by the reaction

$$RE_2SiO_5 + SiO_2 \rightarrow RE_2Si_2O_7. \quad (3)$$

In our case, the reaction is completed at 1300 °C.

In Fig. 4a, we plot the excitation spectra for the sample heated at 1300 °C, obtained by monitoring the emission at the energies corresponding to two maximums of the $^5D_0 \rightarrow {}^7F_1$ emission transition (593 and 594.5 nm). As shown, the spectra slightly differ in the range of *f–f* transitions, but the most pronounced difference refers to the position of CT bands. They are located at 230 and 255 nm proving two different crystallographic sites for Eu^{3+} ions in the lattice.

Fig. 4b presents the $^5D_0 \rightarrow {}^7F_1$ emission spectra recorded by exciting the sample at 205, 230 and 255 nm. Two components of the $^5D_0 \rightarrow {}^7F_0$ transition in the spectrum obtained exciting the sample at 230 nm are consistent with two different environments of the Eu^{3+} ions. One of these sites can be selectively excited at its CT band at 255 nm. Then, we obtain a set of transitions that very well overlap the low energetic components of the bands of the first spectrum. The higher energetic site cannot be selectively excited because the excitation energy is in part transferred to the lower energetic Eu^{3+} symmetry center and as a result we obtain the emission from both centers. Since

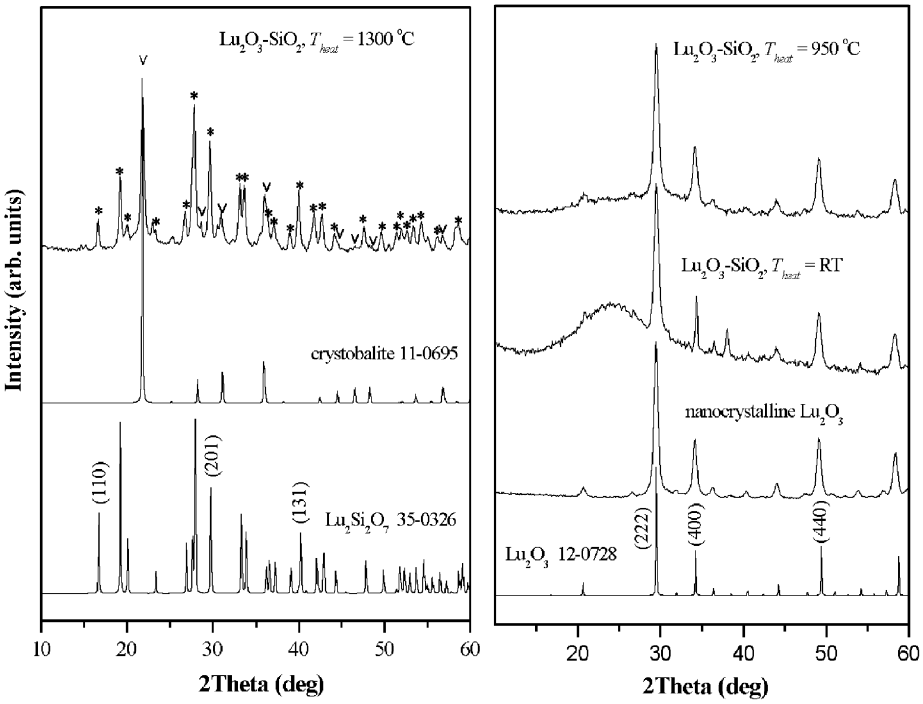

Fig. 3. X-ray patterns of the sample (1) treated at different temperatures. The spectrum of nanocrystalline Lu_2O_3:Eu^{3+} is included for comparison. * Indicates the peaks related to $Lu_2Si_2O_7$, v indicates the peaks related to crystobalite.

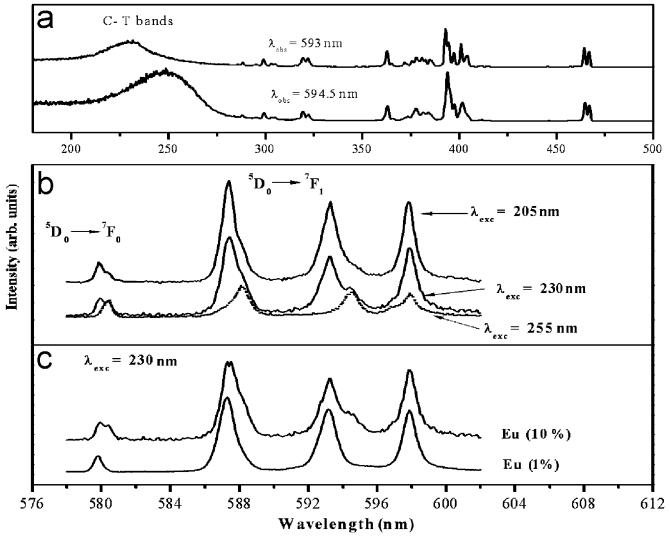

Fig. 4. Excitation spectra of the sample (1) (a), the $^5D_0 \rightarrow {}^7F_{0,1}$ emission spectra of the sample (1) for different excitation energies (b), $^5D_0 \rightarrow {}^7F_{0,1}$ emission spectra of the sample (1) for different concentration of the activator (c). The sample was heated at 1300 °C.

excitation at the maximum of the CT band leads in fact to excitation of both centers simultaneously, to ensure that the energy transfer is the case we excited the sample at the higher energetic edge (205 nm) of the CT band of the higher energetic component, beyond the range of the lower energetic CT band. As we can see, the emission from both centers is still observed. It is worth noting that the energy transfer between different symmetry centers is promoted by increasing concentration of the active ions [4] and has been expected for our relatively high concentrated sample (10%). To prove this deduction and find out which Eu^{3+} center is created as the first by simple substitution of the Lu^{3+} ions, we synthesized the sample containing 1% of the active ions in the lutetium lattice.

In Fig. 4c, we compare $^5D_0 \rightarrow {}^7F_1$ emission spectra of the samples containing 10% and 1% of the Eu^{3+} ions. As presented, the less concentrated sample under 230 nm excitation exhibits the emission corresponding to the higher energetic Eu^{3+} site. The lower energetic site was not detected for concentration of 1%. We cannot treat quantitatively the relation between the energy transfer and the concentration of the active ions at this stage of investigation. It will be examined in the future.

The presence of Eu^{3+} in different crystallographic sites was also evaluated by Raman spectroscopy. The room temperature Raman spectra of the samples calcined at 1300 °C, containing 1 and 10% mol of Eu^{3+} are shown in Fig. 5. One can note that the bands for the sample of higher concentration exhibit an inhomogeneous broadening and a shift towards lower frequencies as compared to the sample containing 1% mol of Eu^{3+}. Note also the appearance of the two additional bands at 145 and 368 cm^{-1}. The above observations are consistent with the change in the coordination of Eu^{3+} deduced basing on electron spectroscopy.

To understand the nature of these two emitting centers, one has to investigate the crystal structure of $Lu_2Si_2O_7$.

Lutetium pyrosilicate crystallizes in $C2/m$ symmetry group. Its crystal lattice can be described as a stacking of

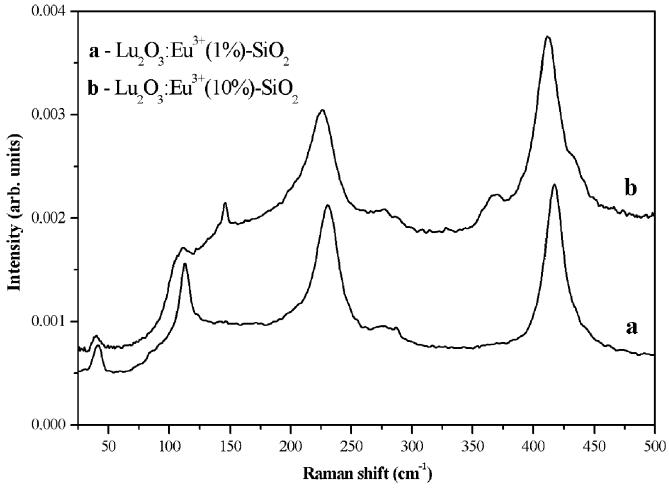

Fig. 5. Room temperature Raman spectra of the Lu_2O_3:Eu^{3+}–SiO_2 ceramics calcined at 1300 °C, containing 1 and 10 mol% of Eu^{3+}.

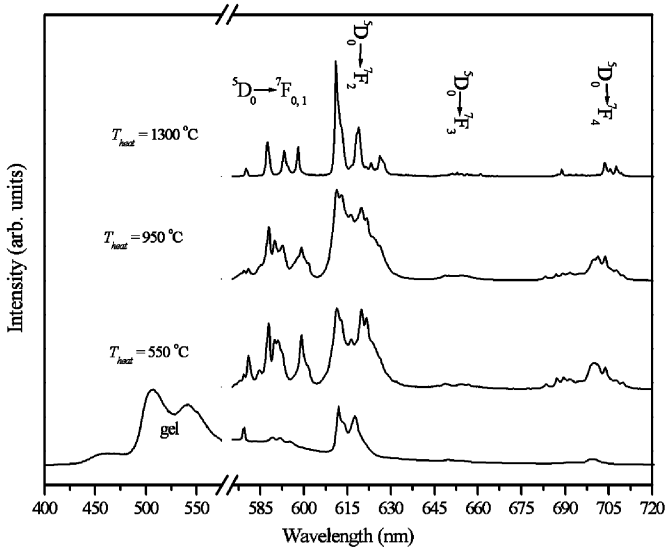

Fig. 6. Luminescence spectra of the sample (2) treated at different temperatures.

alternating parallel layers of [LuO_6] octahedral sharing edges, and of isolated [Si_2O_7] groups. [Si_2O_7] groups are formed by two [SiO_4] tetrahedra sharing one oxygen and the Si–O–Si bond angle between tetrahedra is equal to 180° [19]. The lattice offers only one crystallographic site for the doping lanthanide ion. Yan et al. [18] demonstrated the Ce^{3+} (3%) activated $Lu_2Si_2O_7$ single-crystal luminescence originated from the only one Ce^{3+} emitting center. Because the ionic radius of Ce^{3+} ion is larger then Lu^{3+} one (1.034 and 0.85 Å, respectively), high level of doping is rather impossible (segregation coefficient determined by the authors equal to 0.38). The ionic radius of Eu^{3+} ion (0.95 Å) is between Ce^{3+} and Lu^{3+} radii and similarly one cannot expect the incorporation of large amount of Eu^{3+} ions to the $Lu_2Si_2O_7$ network without introducing any perturbation. In fact, 10% doping forces the excess of the Eu^{3+} ions to occupy positions in the crystal structure having the lattice constants changed. Moreover, the excess ions do not enter the lattice randomly, but occupy the same lower energetic crystallographic site.

It is worth noting that contrary to the monocrystal grown by the Czochralski technique, the procedure applied by us allows much higher level of the activator doping, the excess ions are located in the second crystallographic site.

A good measure of the asymmetry of the coordination polyhedron around the Eu^{3+} ions is the ratio of the integrated intensities of the $^5D_0 \rightarrow {}^7F_1$ and $^5D_0 \rightarrow {}^7F_2$ emission transitions:

$$R = \frac{I(^5D_0 \rightarrow {}^7F_1)}{I(^5D_0 \rightarrow {}^7F_2)}. \quad (4)$$

The R values are 0.4 and 0.34 for the higher and lower energetic spectra, respectively. The decrease of the R value with increasing europium concentration indicates higher distortion of the coordination sphere of the lower energetic Eu^{3+} center.

Fig. 6 presents the emission spectra of the sample (2) excited at 250 nm in the CT band. Contrary to the sample (1), even unheated sample exhibits the spectrum that is different from that for crystalline Lu_2O_3:Eu^{3+}. Additionally, a broad emission band of the matrix origin appears at the green region of the spectrum. The emissive properties of xerogels are known and reported by many authors [31,32] and also by us [33]. The samples heated at higher temperatures do not show the matrix emission and their spectra differ from each other presenting gradual conversion of Lu_2O_3 to the final form represented by the spectrum of the sample heated at 1300 °C. Please note that the spectra for the samples dried at ambient, 550 and 950 °C temperatures are composed of broad bands characteristic for amorphous surrounding of the emitting ions. At 1300 °C, the lanthanide environment becomes crystalline, which is reflected by the narrow bands of Eu^{3+} emission. Moreover, the spectrum is identical to that taken for the sample (1) heated at 1300 °C. It is evident that irrespective of transformations the samples underwent at temperatures below 1300 °C, they finally become the same crystalline material at 1300 °C, namely $Lu_2Si_2O_7$. Fig. 7 shows the evolution of the CT transition with increasing temperature for the sample containing 1% of the Eu^{3+} ions. As we see, the sample heated at 550 °C is represented by a broad CT band, centered at 250 nm. Broadening is characteristic for different though similar amorphous environments of the Eu^{3+} ions. Similarly, the sample heated at 950 °C exhibits broad CT bands, but shifted to higher energies, which proves the evolution of the amorphous phases with creation of stronger Eu–O bonds. The visible tail at the low energetic edge of the CT band represents an unconverted form that dominates at 550 °C. At 1300 °C, the CT band becomes narrower with maximum at 230 nm, being consistent with the presence of the only one crystalline form of $Lu_2Si_2O_7$.

To understand the transformations the sample (2) underwent with increasing temperature, it is reasonable

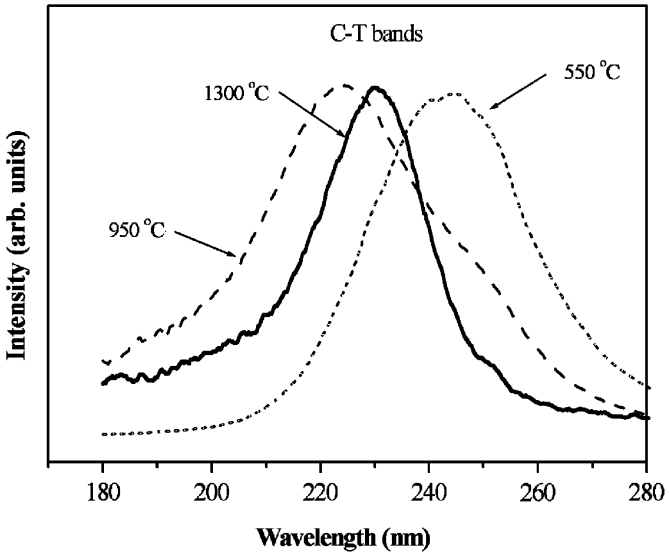

Fig. 7. The *C–T* bands of the sample (2) treated at different temperatures.

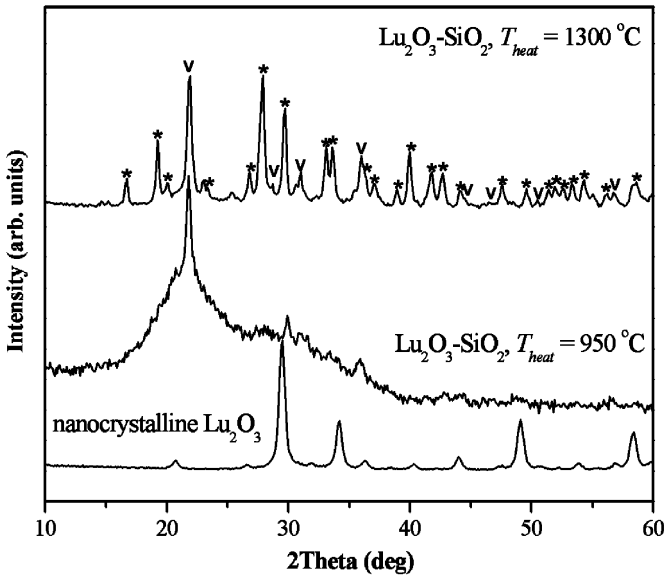

Fig. 8. X-ray patterns of the sample (2) treated at different temperatures. The spectrum of nanocrystalline Lu_2O_3:Eu^{3+} is included for comparison. ∗ indicates the peaks related to $Lu_2Si_2O_7$, v indicates the peaks related to crystobalite.

to correlate the emission spectra with the respective XRD patterns.

In Fig. 8, we present XRD patterns for the sample (2) heated at indicated temperatures. It is seen that at 950 °C the sample is composed of amorphous silica, crystobalite and only traces of crystalline Lu_2O_3. It means that most of the Ln^{3+} ions are dispersed within amorphous phase of SiO_2 matrix. Please note that for the sample (1) at those temperatures Lu_2O_3 exists as the only crystalline form.

For the sample heated at 1300 °C, we detected exactly the same XRD pattern as for the sample (1).

Hreniak et al. [16] previously reported on optical and structural properties of Lu_2O_3:Eu^{3+} embedded in sol–gel derived SiO_2 matrix. They also proved a structural transformation of lutetium oxide (800 °C) to pyrosilicate (1350 °C). However, the authors recorded almost identical emission spectra for the sample treated at both indicated temperatures. Moreover, wide bands of the recorded spectra correspond to amorphous phase. In our case, the emission spectrum for pyrosilicate meaningly differs from those recorded for lower temperatures and is consistent with the spectrum for single crystal [34]. Narrow bands of the spectra represent crystalline phases.

In Fig. 9, we show luminescence spectra of the sample (1) excited with X-rays. Independent of the heating temperature, the radioluminescence results exclusively from radiative recombination of excited electrons within the Eu^{3+} ions. Please note that the samples do not exhibit afterglow accompanying the main emission. The highest emission intensity has been recorded for the sample heated at 950 °C, and the smallest for the sample treated at 1300 °C. This result proves that materials heated at, and below 950 °C can be considered as potential phosphors for X-ray imaging, while those treated at higher temperatures can find application as a cathode-ray phosphor.

Table 1 groups the emission decay times for both samples measured at ambient and 77 K temperatures. The decay times for nanocrystalline Lu_2O_3:Eu^{3+} are provided for comparison.

With the exception of the higher concentrated sample (10%), the curves measured were exponential.

As we can see, the general trend is that the decay times become longer with increasing temperature of thermal treatment. This is due to rather high content of hydroxyl and organic groups in the xerogel. As it was mentioned above, rising temperature leads to pronounced reduction of the content of water and organic molecules in gel. This in turn diminishes the multiphonon relaxation process that quenches the emission. However, the decay times for the sample (1) before heat treatment are shorter than the respective values for powder. Please note that for the sample (2), where we deal with a new, better shielding surrounding of the lanthanide ions, the decay times are slightly longer. At 1300 °C, both samples are fully converted to pyrosilicate. For the higher concentrated sample we recorded two components of the decay time, corresponding to two symmetry sites of the Eu^{3+} ion. The longer ones are almost identical to the decay times for the lower concentrated sample and can be related to the higher symmetry site (see discussion above). Please note that the same lifetimes for the sample of different concentration could evidence the lack of energy transfer between two Eu^{3+} symmetry centers, proved by the emission spectra. However, according to the excitation spectra, the 355 nm laser line excites Eu^{3+} in both centers and one cannot deduce about the energy transfer. It is worth noting that the lifetimes for the $Lu_2Si_2O_7$:Eu^{3+} single crystal reported by Bretheau-Raynal et al. [34] were below 2 ms. It is

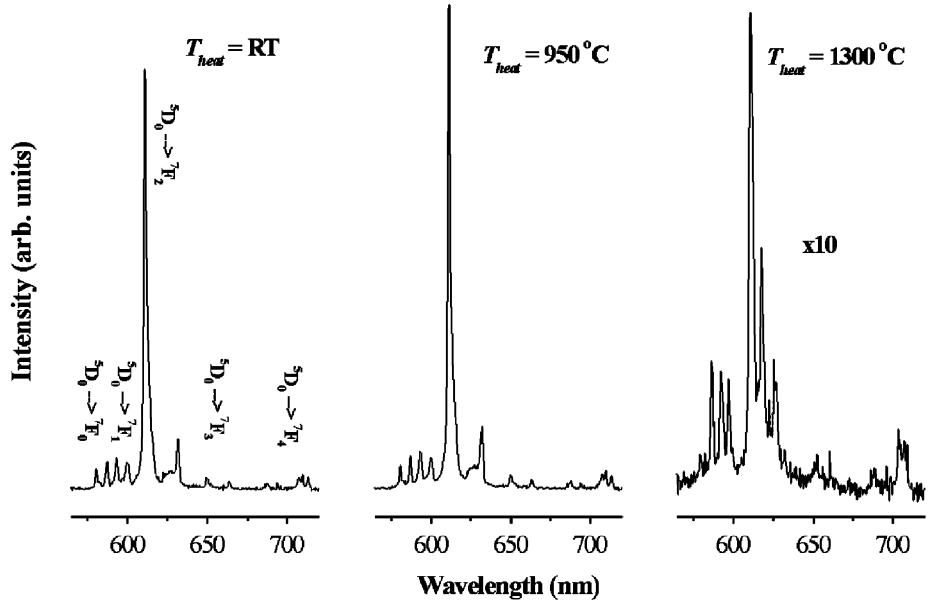

Fig. 9. Room temperature emission spectra under X-ray excitation of $Lu_2O_3:Eu^{3+}$(10%)/SiO_2 ceramics obtained by the sol–gel technique.

Table 1
Emission decay times for $Lu_2O_3:Eu^{3+}$ nanocrystallites and $Lu_2O_3:Eu^{3+}$ embedded in silica matrix

T_{heat} (°C)	Sample (1)				Sample (2)	
	τ_{RT} (ms)		τ_{77} (ms)		τ_{RT} (ms)	τ_{77} (ms)
RT	0.9		1.02		1.25	1.41
550	1.54		1.49		1.89	1.83
950	1.35		1.63		2.11	2.19
1300 (10% Eu^{3+})	2.26	0.45	2.23	0.47		
1300 (1% Eu^{3+})	2.26		2.3			
Nanocrystalline $Lu_2O_3:Eu^{3+}$	1.2		1.35			

$\lambda_{exc} = 355$ nm.
τ_{RT}: decay time measured at room temperature; τ_{77}: decay time measured at 77 K; RT: room temperature.

interesting to note that the decay times for pyrosilicate do not exhibit temperature dependence.

4. Conclusions

Optical properties of nanosized $Lu_2O_3:Eu^{3+}$ obtained by the combustion synthesis can be preserved in the sol–gel derived silica matrix heated up to 950 °C. Those materials exhibit very effective radioluminescence and no afterglow and are very promising as phosphors for X-ray imaging.

Independently of the synthesis procedure, lutetium pyrosilicate is formed as a final product and the reaction is completed at 1300 °C. Pyrosilicate exists as the only lanthanide nanocrystallite. Applied synthesis procedure allows much higher level of the activator doping compared to the monocrystals grown by the Czochralski technique. It was proved that the Eu^{3+} ions occupy the only one symmetry center for lower concentration (1%) of the activator and two for higher concentration (10%).

Eu^{3+} doped lutetium pyrosilicate obtained by the procedure applied by us is characterized by very effective emission and decay time longer than 2 ms. Optical properties of the material makes it a good material for a cathodoluminescent phosphor.

Acknowledgment

Financial support from the Polish Committee for Scientific Research (KBN, Grant no. 20401331/0289) is gratefully acknowledged.

References

[1] G.C. Tyrrell, Nucl. Instrum. Methods A 546 (2005) 180.
[2] A. Garcia-Murillo, C. Le Luyer, C. Dujardin, T. Martin, C. Garapon, C. Pedrini, J. Mugnier, Nucl. Instrum. Methods A 486 (2002) 181.
[3] B.M. Tissue, Chem. Mater. 10 (1998) 2837.
[4] E. Zych, J. Phys.: Condens. Matter 14 (2002) 5637.
[5] Q. Li, L. Gao, D. Yan, Nanostruct. Mater. 8 (1997) 825.
[6] L.E. Shea, J. McKittrick, O.A. Lopez, E. Sluzky, J. Am. Ceram. Soc. 79 (1996) 3257.
[7] V. Sudarsan, S. Sivakumar, F.C.J.M. van Veggel, M. Raudsepp, Chem. Mater. 17 (2005) 4736.
[8] L. Zhou, B. Yan, Inorg. Mater. 41 (2005) 613.
[9] J. Dhanaraj, R. Jagannathan, T.R.N. Kutty, C.-H. Lu, J. Phys. Chem. B 105 (2001) 11098.
[10] C. Cannas, M. Mainas, A. Musinu, G. Piccaluga, A. Speghini, M. Bettinelli, Opt. Mater. 27 (2005) 1506.
[11] G. Xia, S. Zhou, J. Zhang, S. Wang, Y. Liu, J. Xu, J. Cryst. Growth 283 (2005) 257.
[12] E. Zych, J. Phys.: Condens. Matter 14 (2002) 5637.

[13] FIZ Karlsruhe & Gmelin Inst., 1990 ICSD Collection Code 40471, release 99/1.
[14] A. Saiki, N. Ishizawa N. Mizutani, M. Kato, Acta Crystallogr. 40 (1984) 76.
[15] A. Garcia-Murillo, C. Le Luyer-Urlacher, C. Dujardin, C. Pedrini, J. Mugnier, J. Sol–Gel Sci. Tech. 26 (2003) 957.
[16] D. Hreniak, E. Zych, L. Kępiński, W. Stręk, J. Phys. Chem. Solids 64 (2003) 111.
[17] C. Yan, G. Zhao, Y. Hang, L. Zhang, J. Xu, Mater. Lett. 60 (2006) 1960.
[18] C. Yan, G. Zhao, Y. Hang, L. Zhang, J. Xu, J. Cryst. Growth 281 (2005) 411.
[19] D. Pauwels, et al., US Patent Specification, 2002, 6437336.
[20] D. Pauwels, et al., IEEE Trans. Nucl. Sci. 51 (2004) 1084.
[21] M. Daldosso, J. Sokolnicki, L. Kepinski, J. Legendziewicz, A. Speghini, M. Bettinelli, J. Lumin. 122–123 (2007) 858.
[22] C.J. Brinker, G.W. Scherer, Sol–Gel Science, Academic Press, Boston, 1990.
[23] J. Legendziewicz, W. Stręk, J. Sokolnicki, B. Keller, M. Borzechowska, Acta Phys. Pol. 90 (2) (1996) 461.
[24] W. Stręk, J. Sokolnicki, B. Keller, M. Borzechowska, J. Legendziewicz, Proc. SPIE 3176 (1997) 259.
[25] J. Sokolnicki, J. Legendziewicz, K. Maruszewski, W. Stręk, J. Sol–Gel Sci. Technol. 13 (1998) 611.
[26] W. Stręk, J. Legendziewicz, E. Łukowiak, K. Maruszewski, J. Sokolnicki, A.A. Boiko, M. Borzechowska, Spectrochim. Acta, Part A 54 (1998) 2215.
[27] J. Legendziewicz, W. Stręk, J. Sokolnicki, D. Hreniak, V. Zolin, Opt. Mater. 19 (2002) 175.
[28] M. Xu, W. Zhang, N. Dong, Y. Jiang. Y. Tao, M. Yin, J. Solid State Chem. 178 (2005) 477.
[29] J. Legendziewicz, J. Alloys Compds. 341 (2002) 34.
[30] N. Maier, G. Rixecker, K.G. Nickel, J. Solid State Chem. 179 (2006) 1630.
[31] J. Lin, K. Baerner, Mater. Lett. 46 (2000) 86.
[32] J. Garcia M., M.A. Mondragon, C. Tellez S., A. Camparo, V.M. Castano, Mater. Chem. Phys. 41 (1995) 15.
[33] J. Sokolnicki, J. Legendziewicz, G. Muller, J.P. Riehl, Opt. Mater. 27 (2005) 1529.
[34] F. Bretheau-Raynal, N. Tercier, B. Blanzat, M. Drifford, Mater. Res. Bull. 15 (1980) 639.